

Off-axis electron holography of manganite-based heterojunctions: Interface potential and charge distribution*

Zhi-Bin Ling(令志斌)[†], Gui-Ju Liu(刘桂菊)[†], Cheng-Peng Yang(杨成鹏),
Wen-Shuang Liang(梁文双), and Yi-Qian Wang(王乙潜)[‡]

College of Physics & State Key Laboratory, Qingdao University, Qingdao 266071, China

(Received 11 January 2019; revised manuscript received 13 February 2019; published online 5 March 2019)

The interfacial electrical potentials and charge distributions of two manganite-based heterojunctions, *i.e.*, $\text{La}_{0.67}\text{Ca}_{0.33}\text{MnO}_3/\text{SrTiO}_3:0.05 \text{ wt\% Nb}$ (LCMO/STON) and $\text{La}_{0.67}\text{Ca}_{0.33}\text{MnO}_3/\text{LaMnO}_3/\text{SrTiO}_3:0.05 \text{ wt\% Nb}$ (simplified as LCMO/LMO/STON), are studied by means of off-axis electron holography in a transmission electron microscope. The influences of buffer layer on the microstructure and magnetic properties of the LCMO films are explored. The results show that when a buffer layer of LaMnO_3 is introduced, the tensile strain between the STON substrate and LCMO film reduces, misfit dislocation density decreases near the interfaces of the heterojunctions, and a positive magnetoresistance is observed. For the LCMO/STON junction, positive and negative charges accumulate near the interface between the substrate and the film. For the LCMO/LMO/STON junction, a complex charge distribution takes place across the interface, where notable negative charges accumulate. The difference between the charge distributions near the interface may shed light on the observed generation of positive magnetoresistance in the junction with a buffer layer.

Keywords: $\text{La}_{0.67}\text{Ca}_{0.33}\text{MnO}_3$ films, electron holography, magnetic properties, interfacial electrical potential, charge distribution

PACS: 61.05.jp, 68.37.-d, 68.37.Og, 75.70.Cn

DOI: 10.1088/1674-1056/28/4/046101

1. Introduction

Manganite perovskite films are attractive materials due to their colossal magnetoresistance (CMR) effect, excellent magnetic-field-dependent rectifying characteristics and resulting potential applications.^[1–3] In manganite, the strong magnetic-conductive coupling^[4] and order–disorder transition of the spin, orbital, and charge degree of freedom^[5] are severely depressed at a junction by strong interface/surface effect. Thus, the interfacial behavior has an important influence on the properties of thin-film heterojunctions and related devices.

The novel physical phenomena in CMR materials usually occur in interfacial regions, so it is reasonable to believe that the creation of multilayer heterostructures by the insertion of a buffer layer will allow us to tune the physical properties. Yamada *et al.*^[6] found that the interfacial ferromagnetism of a $\text{La}_{0.6}\text{Sr}_{0.4}\text{MnO}_3$ film on SrTiO_3 can be enhanced by the introduction of an LaMnO_3 (LMO) buffer layer. Wei *et al.*^[7] reported that the insertion of LMO layer causes the photovoltaic effect to be weakened for the $\text{La}_{0.67}\text{Ca}_{0.33}\text{MnO}_3/\text{SrTiO}_3:0.05 \text{ wt\% Nb}$ (LCMO/STON) junction. Gao *et al.*^[8] explored the enhanced magnetic field effect in an $\text{La}_{0.5}\text{Ca}_{0.5}\text{MnO}_3$ film on STON by adding an LMO

buffer layer. They found that an appropriate buffer layer can affect the charge carriers, interfacial barrier, depletion width, and further modify the interfacial properties. Manganites can exhibit novel magnetoelectric phenomena by interface modification. However, the physical origin of magnetoelectricity phenomenon is not clear and needs further study. Understanding the energy barriers, charge distribution and their relationship with physical properties in these heterojunctions is a crucial issue for both academic research and technological applications. Electron holography based on transmission electron microscopy (TEM) is a promising way to investigate such heterojunctions.^[9] Combined with theoretical analysis, electron holography can directly reveal the distribution of electrostatic potential and the charge accumulation at heterojunctions.^[10–13]

In the present article, two thin film heterojunctions, *i.e.*, LCMO/STON and LCMO/LMO/STON, are investigated in detail. The microstructure of the heterostructure, with and without a buffer layer, are examined by high-resolution transmission electron microscopy (HRTEM). Electrostatic potential and charge distribution near the interface of the heterojunction are identified by off-axis electron holography.

*Project supported by the National Natural Science Foundation of China (Grant No. 10974105), the High-end Foreign Experts Recruitment Programs, China (Grant Nos. GDW20173500154 and GDW20163500110), the Taishan Scholar Program of Shandong Province, Shandong Province “Double-Hundred Talent Plan” on 100 Foreign Experts and 100 Foreign Expert Teams Introduction Project, the Top-notch Innovative Talent Program of Qingdao City, China (Grant No. 13-CX-08), the Qingdao International Center for Semiconductor Photoelectric Nanomaterials, and Shandong Provincial University Key Laboratory of Optoelectrical Material Physics and Devices.

[†]These authors made equal contribution to this work.

[‡]Corresponding author. E-mail: yqwang@qdu.edu.cn

2. Experimental details

The 30-nm-thick LCMO film was prepared on a 0.05 wt% Nb-doped SrTiO₃ substrate by pulsed laser deposition (PLD) technique forming LCMO/STON junction. The LCMO/LMO/STON junction was fabricated by growing first a 2-nm-thick LMO then a 30-nm-thick LCMO on an STON substrate using the PLD technique. During the deposition, the substrate temperature was kept at 700 °C, and the oxygen pressure was kept at 10 Pa for LMO layer and 80 Pa for LCMO layer. The film thickness was controlled by the deposition time.

The TEM and off-axis electron holography observations were carried out with a Philips CM200/FEG TEM that was equipped with an electrostatic biprism. Specimens for TEM and electron holography examinations were prepared by using conventional technique of mechanical polishing and ion thinning. The ion thinning was performed by using a Gatan model 691 precision ion polishing system with a low voltage. The holograms were obtained with a Gatan 749 multiscan charge-coupled device camera, and processed by Gatan Digital Micrograph software with a Holowork package. The x-ray diffraction (XRD) pattern was recorded by using a Bruker D8 Discover x-ray diffractometer (Cu-K α radiation, $\lambda = 1.5406 \text{ \AA}$). The current-voltage (J - V) characteristic was measured by using a superconducting quantum interference device magnetometer equipped with a resistance measurement unit.

3. Results and discussion

Figure 1 shows XRD patterns recorded around the (002) peak of the LCMO/STON junction with and without an LMO buffer layer. It is shown that the LCMO films are of single phase and grow epitaxially on the STON substrates along the c axis. Meanwhile, the introduction of the LMO buffer layer affects the peak position of (002) reflection of the LCMO film, which reflects the change of out-of-plane lattice parameter for the LCMO film. The lattice parameters of bulk LCMO ($a = 3.856 \text{ \AA}$)^[15] are smaller than those of LMO ($a = 3.880 \text{ \AA}$) and STON ($a = 3.905 \text{ \AA}$)^[16] which indicates that the LCMO film experiences an in-plane tensile strain. It can be noticed from Fig. 1 that the (002) peak of LCMO shifts $\sim 0.2^\circ$ to small angle, suggesting that the lattice spacing of LCMO is elongated along the c axis. For the LCMO film without an LMO buffer layer, the out-of-plane lattice spacing is 3.796 \AA , which is less than that of LCMO film with a buffer layer ($\sim 3.823 \text{ \AA}$). This indicates that the residual compressive strain of LCMO film with buffer layer is less than that of LCMO film without a buffer layer. Notably, the lattice strain still exists in the well-relaxed LCMO film with a buffer layer, which is consistent with the XRD result in Fig. 1.

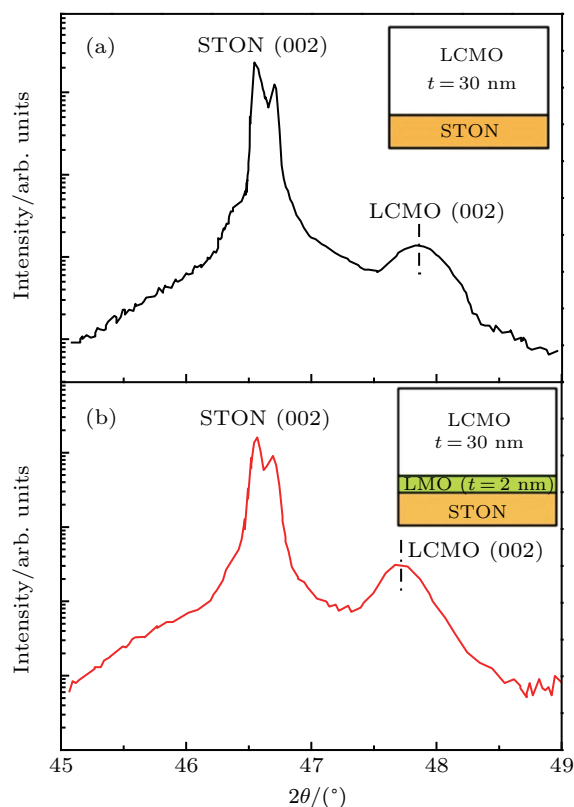


Fig. 1. (a) and (b) XRD pattern of (a) LCMO/STON^[14] (Copyright 2009, American Institute of Physics) and (b) LCMO/LMO/STON junction recorded around (002) peak. Insets show the schematics of the two film junctions.

Figure 2(a) is a typical bright field (BF) TEM image of a cross-sectional LCMO/STON sample with a uniform thickness of $\sim 30 \text{ nm}$. The white arrows indicate the interface between the film and substrate. It can be seen that the interface between the film and substrate is fairly clean and sharp, and the surface is flat without any ripple. Due to the different lattice parameters between STON substrate ($a = 3.905 \text{ \AA}$) and LCMO film ($a = 3.856 \text{ \AA}$), some dislocations are obviously distributed near the interface. Figure 2(b) shows one misfit dislocation near the LCMO/STON interface region. The misfit dislocation is indicated by D, and the extra half atomic plane of this dislocation is indicated by “ \perp ”. It can be seen that the misfit dislocation is not exactly located at the interface but inside the LCMO film a few monolayers away from the interface. To determine the Burgers vector for D, a Burgers circuit is drawn to enclose the dislocation as shown in Fig. 2(b). It can be seen that there is a gap between the starting and ending point of the Burgers circuit as indicated by red arrows. The Burgers vector is determined to be $1/2 [\bar{1}01]$. Figure 2(c) shows a typical BF TEM image of a cross-sectional LCMO/LMO/STON sample with a film thickness of $\sim 30 \text{ nm}$. It can be seen that the interface between film and substrate is flat. Figure 2(d) displays a typical HRTEM image of the LCMO/LMO/STON junction where the interfaces are illustrated by dashed lines. The dislocations in Fig. 2(d) are less than those in Fig. 2(b), which demonstrates that the introduction of LMO buffer layer can

effectively reduce the dislocations around the interface of the heterojunction. The difference in lattice parameter between substrate and film evokes the lattice mismatch near the interface. In other words, the bigger the difference in lattice parameter, the larger the lattice mismatch will be. Because the lattice parameter of LMO ($a = 3.880 \text{ \AA}$) buffer layer is slightly larger than that of LCMO ($a = 3.856 \text{ \AA}$) film and is smaller than that of STON ($a = 3.905 \text{ \AA}$) substrate, there is less lattice mismatch near the interface between LCMO film and LMO buffer layer, indicating that lattice strain in the LCMO/LMO/STON heterojunction is less than that in LCMO/STON. When the films are epitaxially grown on the substrates, lattice strain will generate at the interface due to the existence of lattice mismatch. The appearance of dislocations near the interface can partially reduce the lattice strain in the film. The larger the lattice strain, the more the dislocations are. Introducing a buffer layer can reduce the lattice strain in the film, which will effectively reduce the formation of dislocations near the interfaces in LCMO/LMO/STON.

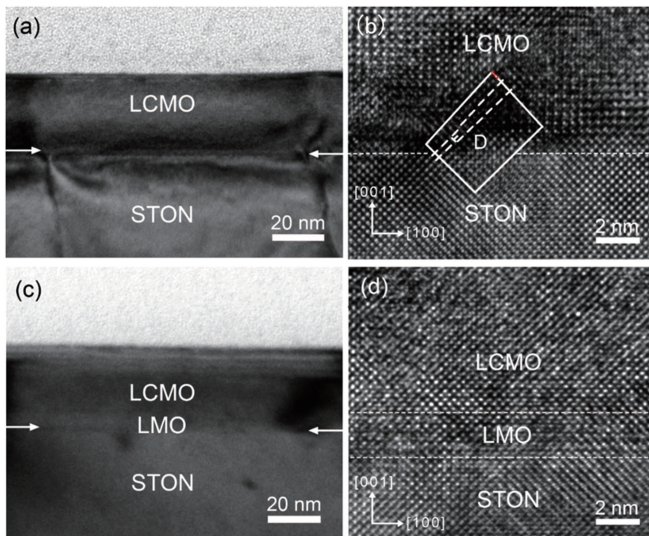


Fig. 2. (a) Typical cross-sectional BF TEM image and (b) HRTEM image of LCMO/STON film junction. (c) Typical cross-sectional BF TEM image and (d) HRTEM image of LCMO/LMO/STON film junction.

Figure 3 shows typical semilogarithmic J - V curves of LCMO/STON junction with a 2-nm-thick LMO buffer layer. As observed in the literature,^[17] a linear relationship between $\log J$ and V is found for the junctions with an LMO buffer layer. As the temperature decreases, the $\log J$ - V curve shifts to a high bias voltage direction and its slope increases. However, the $\log J$ - V curves of LCMO/LMO/STON exhibit an obvious downward shift when exerting a magnetic field, indicating a positive magnetoresistance (MR) effect, which is completely different from the negative MR effect observed in the conventional manganite junctions without a buffer layer.^[18] The physical properties of a material are determined by its microstructure, thus the appearance of the positive MR might be

associated with the different microstructure of these two heterojunctions, such as the lattice mismatch and misfit dislocations near the interfaces of the junctions. Apart from the effect of lattice strain and dislocations, the electrostatic potential and charge distribution around the interface region can affect the MR of LCMO films. Hence, it is necessary to study the electrostatic potential and charge distribution near the interface of LCMO/STON and LCMO/LMO/STON heterojunction.

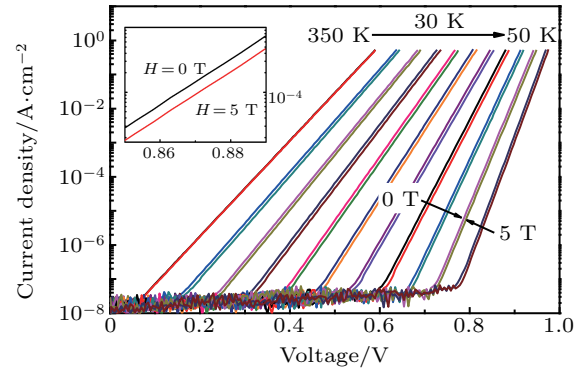


Fig. 3. Semilogarithmic plot of the J - V characteristics of LCMO/LMO(2 nm)/STON junction measured with and without magnetic field. Inset shows magnified parts of the J - V curve in magnetic field.

To determine the influences of the interface on the electrostatic potential and charge density in these heterojunctions, the electron holography is carried out. Figure 4(a) shows a hologram taken from the interface region of LCMO/STON junction under a positive biprism voltage of 80 V. It is recorded slightly off the zone-axis direction to reduce the dynamic effect. Interference fringes with good visibility have an average space (s_f) of about 0.155 nm; thus, the spatial resolution ($\sim 3s_f$) in the reconstructed holograms is better than 0.5 nm. The interface of the heterojunction yields an evident contrast difference as indicated by the black arrows. Figure 4(b) shows a reconstructed phase image from Fig. 4(a) using the Holowork package in Digital Micrograph software,^[19,20] which demonstrates a visible phase change from the substrate to the film. Figure 4(c) illustrates an average phase profile normal to the interface, in which each point is averaged laterally over 30 pixels to improve the signal statistics. It is demonstrated that the phase decreases rapidly in the interfacial region, and reaches a stable value in a region 1 nm away from the interface. This reveals a significant change within a narrow layer around the interface and confirms the presence of a depletion layer with a width of about 2 nm. The phase profiles from the other regions across the interface possess a similar sigmoidal characteristic.

In the interface region, the phase changes are directly associated with the potential barrier and charge distribution. If the sample is not strongly diffractive, then the phase shift of the object wave is given by

$$\varphi(x, y) = C_E [V_0 + V(x, y)] t(x, y), \quad (1)$$

where C_E is an energy-dependent constant [$C_E = 7.295 \times 10^{-3}$ rad/(V·nm) for 200-keV electron], t is the thickness of the sample where electron waves are transmitted and V_0 is the mean inner potential (MIP) of the sample. As the phase profile is obtained, the phase shift and the interfacial potential can be written as

$$V(x, y) = \frac{\varphi(x, y)}{C_E t(x, y)} - V_0, \quad (2)$$

For the LCMO/STON and LCMO/LMO/STON heterojunction, the sample thickness values in the examined areas are about 50 nm, which are determined by electron energy-loss spectroscopy. The MIP for manganese oxide is about 7.6 ± 1.3 V, and for STON is about 7 ± 0.9 V.^[10] The MIP used in calculation is 7.6 V for manganese oxide and 7 V for STON. Figure 4(d) shows the resulting potential profile across the junction after subtracting the inner potential difference (0.6 V) between the film and the substrate. The potential variation is similar to the phase profile, which drops to a certain value and then keeps stable. We fit the potential profile with a sigmoidal function of Boltzmann model [Fig. 5(a)] and obtain a barrier height of about -0.92 V between the LCMO film and the STON substrate, as demonstrated by the dashed lines.

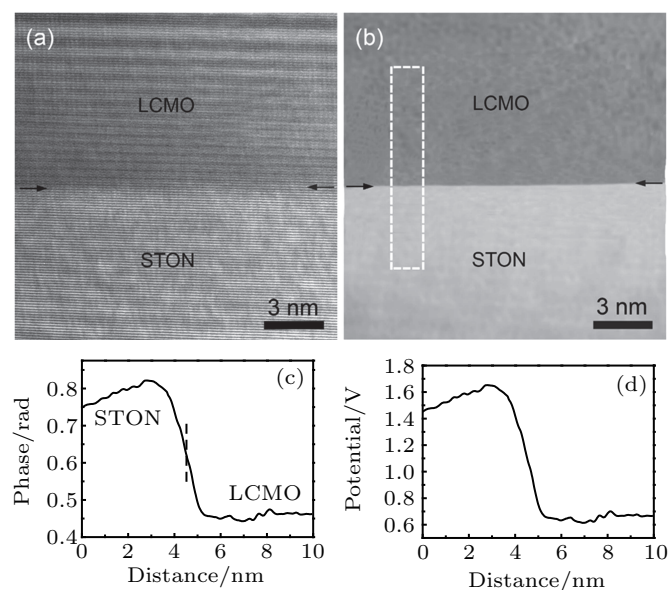


Fig. 4. (a) Hologram taken from the interface region at 300 K. (b) Reconstructed phase image from hologram. (c) Phase profile showing the phase change across LCMO/STON interface. (d) Potential profile across heterojunction after subtracting MIP difference from the phase profile.

According to the relationship among potential distribution, electric field $E(x) = -dV/dx$, and charge density $\rho(x)$, the charge distribution at the interface can be deduced from Poisson's equation

$$\rho(x) = -(\epsilon\epsilon_0) \frac{\partial^2 V(x)}{\partial x^2}, \quad (3)$$

where ϵ is the relative permittivity and ϵ_0 is the permittivity of vacuum. Figure 5(b) shows the corresponding charge distribution obtained from Poisson's equation. It is notable that

positive charges accumulate in the STON substrate within a distance of ~ 2 nm from the interface, and negative charges accumulate in the LCMO film within a distance of ~ 2 nm from the interface. Figure 5(d) shows a simplified illustration displaying the positive charges in the STON substrate and negative charges in the LCMO film. It is known that the Fermi level (E_F) of LCMO is lower than that of STON.^[21] Therefore, when these two materials are in contact with each other, the electrons will migrate from high- E_F STON to low- E_F LCMO, leading to the downward-shift of E_F for STON and the upward-shift of E_F for LCMO until the E_F is lined up on the same level at the interface, which results in accumulation of negative charges in LCMO and positive holes in STON, and produces band bending at the interface. Actually, when two different semiconductors are brought into contact with each other, due to the difference in dielectric constant, bandgap and E_F , the energy band is usually not continuous at the interface.^[22] A schematic diagram showing the band structure of an LCMO/STON junction is given in Figure 5(c). As reported, the bandgap is 3.2 eV for STON and 1.0 eV for LCMO.^[23]

To obtain a comprehensive understanding of the interface influence on potential and charge distribution, an electron holography study is also performed on the LCMO/STON junction with a 2-nm-thick LMO buffer layer. Figure 6(a) is a hologram taken from the interface region of LCMO/LMO/STON under a positive bias potential of 80 V. To determine the locations of interfaces among LCMO, LMO, and STON, we first mark the interfacial locations in the TEM image of LCMO/LMO/STON heterojunction, and then obtain the hologram image of the heterojunction at the same magnification. Thus, we can determine the locations of interfaces by comparing the two images. The interfaces are indicated by dashed lines. Figure 6(b) shows a typical area of the reconstructed phase image from an electron hologram. An average line scan from the STON substrate to the LCMO film in the reconstructed phase image shows a peak of the phase profile at the buffer layer and two valleys at the interfaces (indicated by dashed lines) as shown in Fig. 6(c). First, the phase decreases and reaches a minimum value at the interface between substrate and buffer layer. Second, it forms a peak at the buffer layer, and reaches another minimum value at the interface between LMO buffer layer and LCMO film. Lastly, it increases rapidly at the LCMO layer near the interface. According to the phase profile, the width of the depletion layer of this junction is larger than 2 nm, confirming that the incorporation of LMO could lead to an increase of depletion width. It is indicated from Eq. (2) that the phase difference depends on the electrostatic potential and the specimen thickness. Figure 6(d)

shows the potential change normalized by an average specimen thickness of 50 nm, which is coincident with the change of phase profile. In comparison with Fig. 4(d), with the LMO

buffer layer introduced, the potential drop among substrate, buffer layer and film in Fig. 6(d) decreases and the width of depletion layer increases.

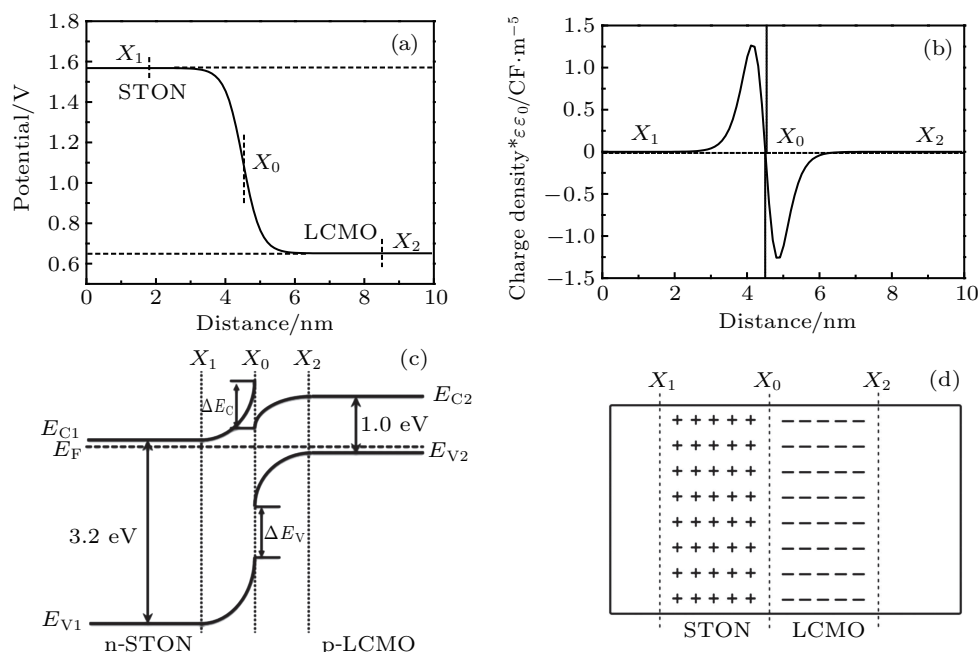


Fig. 5. (a) Fitting profile with a sigmoidal function (Boltzmann model) of potential variations at LCMO/STON interface. (b) Charge density from Poisson's equation. (c) Schematic diagram of energy barrier across heterojunction, showing a discontinuity of electronic bands. (d) Schematic diagram of charge distribution across interface.

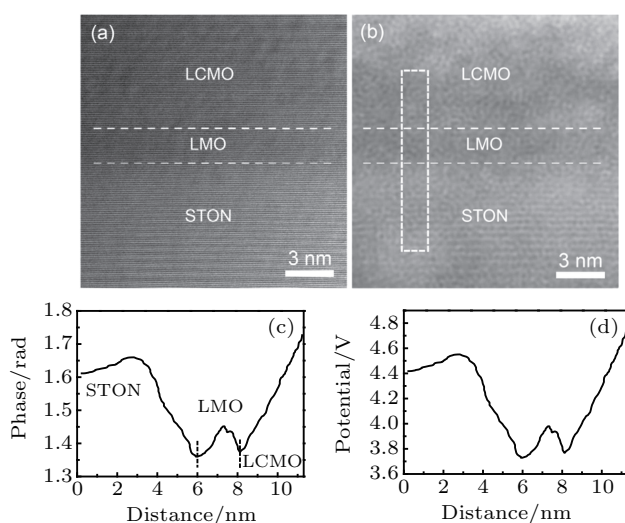


Fig. 6. (a) Hologram taken from interface region at 300 K. (b) Reconstructed phase image from hologram. (c) Phase profile showing peak across the LMO bufferlayer. (d) Potential profile across heterojunction after subtracting MIP difference from phase profile.

Figure 7(a) shows the fitting of Fig. 6(d) with a polynomial function, showing that the potential of LCMO film (0.78 V with respect to the LMO buffer layer) is higher than that of STON substrate (0.55 V with respect to the LMO buffer layer). The potential change profile is in connection with the charge distribution through the Poisson equation. This result directly suggests that certain negative charges are accumulated on the film surface. Figure 7(c) shows the proposed band diagram of LCMO/LMO/STON junction. The bandgap of STON, LMO, and LCMO are 3.2 eV, 1.7 eV, and 1.0 eV,

respectively.^[23,24] The E_F of both STON and LMO are higher than that of LCMO,^[21,25] and the E_V of LMO is lower than that of LCMO and higher than that of STON.^[26] When they contact with each other, electrons will migrate at the interface of LCMO/LMO and LMO/STON, thus producing the band bending at the two interfaces.

The charge distribution can be obtained *via* Eq. (3) based on the potential of Fig. 7(a), and it is shown in Fig. 7(b). It is clear that a small number of negative charges are distributed in the LMO region. Figure 7(d) shows a simplified illustration of the charge distribution, demonstrating that the negative charges accumulate at the two interfacial regions. From Fig. 7(a), it can be noticed that the peak in LMO region is not located in the middle. After measuring the peak position, we find that the charge distribution in the buffer layer can be divided into two regions: the first is ~ 1.5 nm away from the substrate and the second is ~ 0.5 nm away from the film, which is consistent with the phase profile of interface regions in LCMO/LMO/STON junction. From this analysis, it is suggested that the negative charges are preferentially distributed at two interfaces, resulting in a delay of the wave front of exit electron wave function at the interfaces. Manganites are strongly-correlated electron system, in which charge, spin and orbital degrees of freedom are coupled, leading to abundant physical properties. The introduction of a buffer layer in the LCMO/STON junction leads to more complex charge distribution.

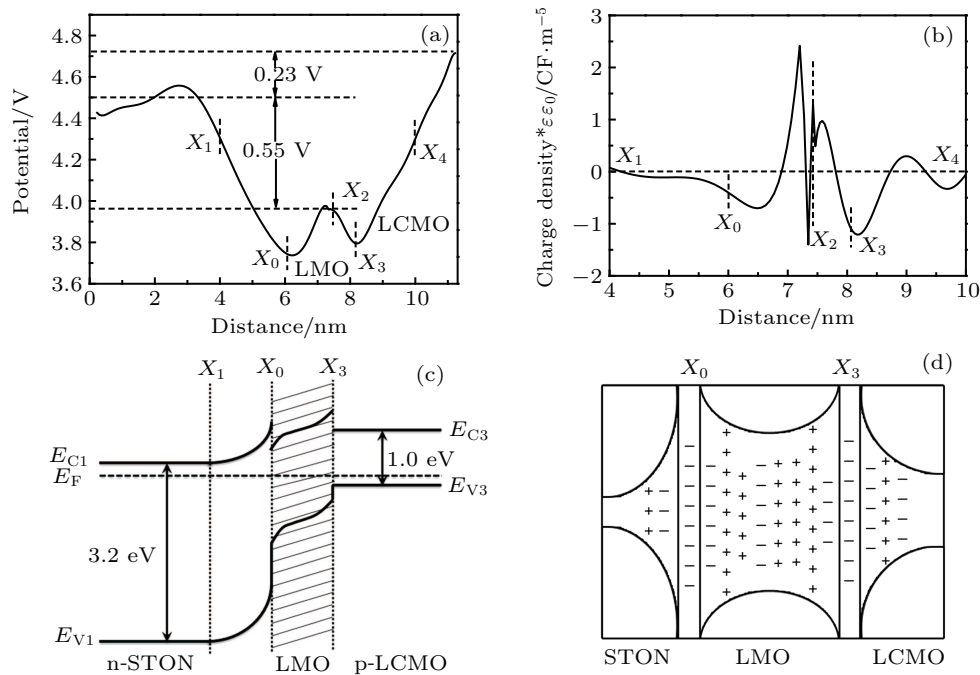


Fig. 7. (a) Fitting profile with polynomial function of potential variation in LCMO/LMO/STON interface. (b) Charge density from Poisson's equation. (c) Schematic diagram of energy barrier across heterojunction. (d) Schematic diagram of charge distribution across interfaces.

4. Conclusions

In this work, the interfacial electrical potential and charge distribution of LCMO/STON and LCMO/LMO/STON heterojunction are investigated by TEM and electron holography. It is found that the introduction of LMO buffer layer reduces the lattice strain between the LCMO film and STON substrate, which leads to the appearance of few misfit dislocations near the interfaces of the junctions. Electron holography examinations indicate that when the LMO buffer layer is introduced, the interfacial potential barrier between the substrate and LCMO film increases and the charge distribution becomes complex. For LCMO/STON, positive and negative charges accumulate symmetrically near the interface on the substrate side and film side, respectively. However, for the junction with a buffer layer, positive and negative charges are distributed asymmetrically and substantial negative charges accumulate on the both sides of the interfaces. This change might be responsible for generating the positive magnetoresistance in LCMO/LMO/STON manganite-based heterojunction.

References

- [1] Xue S, Zhao X L, Wang J L, Tian B B, Huang H, Meng C M, Liu L, Ye L, Sun J L, Meng X J, Zhang X D and Chu J H 2017 *Sci. Chin.-Phys. Mech. Astron.* **60** 027521
- [2] Xie G L, Wang Y H, Yang Y M, Liu H L, Ren T L, Zhu J L, Sun J L and Zhang L W 2011 *Solid State Commun.* **151** 943
- [3] Farokhipoor S, Magén C, Venkatesan S, Íñiguez J, Daumont C J M, Rubi D, Snoeck E, Mostovoy M, de Graaf C, Müller A, Döblinger M, Scheu C and Noheda B 2014 *Nature* **515** 379
- [4] Tanaka H, Zhang J and Kawai T 2001 *Phys. Rev. Lett.* **88** 027204
- [5] Turcaud J A, Pereira A M and Cohen L F 2015 *Phys. Rev. B* **91** 134410
- [6] Yamada H, Ogawa Y, Ishii Y, Sato H, Kawasaki M, Akoh H and Tokura Y 2004 *Science* **305** 646
- [7] Wei A D, Sun J R, Lü W M and Shen B G 2009 *Appl. Phys. Lett.* **95** 052502
- [8] Gao W W, Sun J R, Lu X Y, Shang D S, Wang J, Hu F X and Shen B G 2011 *J. Appl. Phys.* **109** 07C729
- [9] Zhang Z, Zhu T, Feng Y Q and Zhang Z 2005 *Acta Phys. Sin.* **54** 5861 (in Chinese)
- [10] Tian H F, Sun J R, Lü H B, Jin K J, Yang H X, Yu H C and Li J Q 2005 *Appl. Phys. Lett.* **87** 164102
- [11] Gan Z F, Perea D E, Yoo J, He Y, Colby R J, Barker J E, Gu M, Mao S X, Wang C M, Picraux S T, Smith D J and McCartney M R 2016 *J. Appl. Phys.* **120** 104301
- [12] Chalasani R, Pekin A, Rabkin A, Abutbul R E, Dieguez O, Kauffmann Y, Golan Y and Kohn A 2017 *Nano Lett.* **17** 2778
- [13] Nakamura M, Kagawa F, Tanigaki T, Park H S, Matsuda T, Shindo D, Tokura Y and Kawasaki M 2016 *Phys. Rev. Lett.* **116** 156801
- [14] Liang S, Sun J R, Wang J and Shen B G 2009 *Appl. Phys. Lett.* **95** 182509
- [15] Yan L, Niu H J, Duong Giap V, Suchomel M R, Bacsa J, Chalker P R, Hadermann J, van Tendeloo G and Rosseinsky M J 2011 *Chem. Sci.* **2** 261
- [16] Lü W M, Sun J R, Wang J and Shen B G 2009 *Appl. Phys. Lett.* **95** 142107
- [17] Lü W M, Sun J R, Chen Y Z, Shang D S and Shen B G 2009 *Appl. Phys. Lett.* **95** 232514
- [18] Wang D J, Sun J R, Xie Y W, Li Y B, Zhang L G, Wang R W and Shen B G 2010 *Appl. Phys. Lett.* **97** 192503
- [19] Dai T, Liu Y Z and Zhang Z 2006 *Acta Phys. Sin.* **55** 5829 (in Chinese)
- [20] Wang Y, Zhang Z, Zeng Z M and Han X F 2006 *Acta Phys. Sin.* **55** 1148 (in Chinese)
- [21] Lü W M, Sun J R, Wang D J, Xie Y W, Liang S, Chen Y Z and Shen B G 2008 *Appl. Phys. Lett.* **92** 062503
- [22] Gao W W 2012 "Study on electrical, magnetic and photoelectric properties of manganese oxide ultrathin films and their heterojunction", Ph. D. Dissertation (Beijing: Graduate School of Chinese Academy of Sciences) (in Chinese)
- [23] Wang S, Ma Z Z, Xiong J J, Li C J, Hou Y H, Ma T X, Xiong C M, Dou R F and Nie J C 2016 *Appl. Phys. Lett.* **109** 251601
- [24] Liang Y M, Ning X K, Wang Z J, He B, Bai Y, Zhao X G, Liu W and Zhang Z D 2017 *J. Phys. Chem. C* **121** 16810
- [25] Park J H, Chen C T, Cheong S W, Bao W, Meigs G, Chakarian V and Idzerda Y U 1996 *Phys. Rev. Lett.* **76** 4215
- [26] Saitoh T, Bocquet A E, Mizokawa T, Namatame H, Fujimori A, Abbate M, Takeda Y and Takano M 1995 *Phys. Rev. B* **51** 13942